
HEAT AND MASS TRANSFER
AND PHYSICAL GASDYNAMICS

A Model for Calculating the Three Components of the Excess for the Turbulent Field of Flow Velocity in a Round Pipe Rotating about Its Longitudinal Axis

A. F. Kurbatskii* and S. V. Poroseva**

* *Institute of Theoretical and Applied Mechanics, Siberian Division, Russian Academy of Sciences,
Novosibirsk, 630090 Russia*

** *Novosibirsk State University, Novosibirsk, 630090 Russia*

Received December 1, 1995

Abstract—A gradient transfer model is presented for calculating three components of the excess of the turbulent velocity field formed of steady-state flow in a straight round pipe rotating about its longitudinal axis. The coefficients of excess calculated for different values of the parameter of flow swirling agree adequately with the experimental data.

1. INTRODUCTION

The data on the behavior of turbulence spectra and linear scales in a fully developed turbulent flow of incompressible fluid may be derived from a two-point correlation velocity tensor. The system of equations constructed for this tensor is characterized by infinite linking [1]. One of the possible ways of closing such a system of momental equations consists in applying the Millionshchikov hypothesis of quasi-normality [2]. According to this hypothesis, the fourth-order correlation functions of the velocity field are expressed through the second-order correlation functions by the formulas that are true for the normal probability distribution of the velocity field in a turbulent flow [2].

The validity of the hypothesis of quasi-normality was verified in a series of experimental studies. In [3], the experimental data were reported for a homogeneous turbulent flow observed behind the honeycomb in a wind tunnel. These data were found to agree well with the hypothesis within the limits of measurement error.

For nonswirling and swirling flows in a straight round pipe, the hypothesis of quasi-normality was tested in the experiments described in [4]. The measurements were performed for both time and space two-point correlation functions of the second and fourth orders for the longitudinal velocity pulsation in the pipe. It was found that the normalized fourth-order correlation functions, calculated according to the Millionshchikov hypothesis through the second-order correlation functions, differed from the measured values by not more than 4% in the vicinity of their peaks and by 12% at the periphery. In swirling flow (the pipe was rotated at a constant rate about its longitudinal axis), the difference between the measured and calculated values was smaller and did not exceed 3%.

The foregoing experimental results suggest the possibility of using the Millionshchikov hypothesis for expressing the normalized fourth-order correlation functions through the second-order correlation functions. However, to express the fourth-order one-point moments through second-order one-point moments, more exact relations are required than those resulting from the Millionshchikov hypothesis of quasi-normality.

In this paper, we present the results of simulation of central fourth-order one-point moments of the velocity field formed in a fully developed turbulent flow inside a straight round pipe.

The model we propose for describing the behavior of the central fourth-order moments in such a flow is constructed on the hierarchical principle. The first and second moments of the velocity field are determined by the model of Reynolds stress transfer. The latter is based on the “standard” model representations used for describing the main mechanisms of transformation of turbulent stresses. Such representations provide a sufficiently good agreement with the experimental data except for the flow region in the immediate vicinity of the pipe wall. The detailed description of this model and the computational results are presented in papers [5–7]. The third-order moments of the velocity field are found from the gradient transfer model described in [6, 7]. This model is based on the use of the first- and second-order moments that are assumed to be known. Therefore, the model developed for describing the fourth-order moments of the velocity field is based on the assumption that all lower-order moments are already determined.

2. EQUATIONS FOR THE FOURTH-ORDER MOMENTS OF THE VELOCITY FIELD IN A FULLY DEVELOPED TURBULENT FLOW IN A ROUND PIPE

We consider a fully developed turbulent flow of incompressible fluid in a straight round pipe. We use the cylindrical coordinate system (r, φ, z) , where z is the coordinate along the pipe axis, r is the coordinate along the pipe radius directed from the axis to the wall, and φ is the azimuth coordinate. The averaged values are given by capital letters, and the turbulent pulsations of the quantities are denoted by small letters.

The angular brackets indicate the average values. The standard procedure of subtracting the Reynolds equations from the Navier–Stokes equations allows us to obtain (see, e.g., Ch. 7 in [8]) the dynamical equations for the velocity pulsations $u_z = \tilde{u}_z - U_z$, $u_r = \tilde{u}_r - U_r$, and $u_\varphi = \tilde{u}_\varphi - U_\varphi$. Using these equations, we can write equation (A1) (see Appendix) for a mixed one-point moment of the velocity field $\langle u_z^{n+1} u_r^{m+1} u_\varphi^{k+1} \rangle$ (n, m , and k are integers).

The equations for the central fourth-order moments $\langle u_z^4 \rangle$, $\langle u_r^4 \rangle$, and $\langle u_\varphi^4 \rangle$ are derived from (A1) for the exponent values of $n = 3, m = k = -1; m = 3, n = k = -1$; and $k = 3, n = m = -1$, respectively. For a fully developed turbulent flow in a round pipe, these equations have the form

$$-\left[\frac{d\langle u_z^4 u_r \rangle}{dr} + \frac{\langle u_z^4 u_r \rangle}{r} \right] - 4\langle u_z^3 u_r \rangle \frac{dU_z}{dr} + \Pi_{zz}^4 - \varepsilon_{zz}^4 + \nu \nabla^2 \langle u_z^4 \rangle + 4 \left[\frac{d\langle u_z u_r \rangle}{dr} + \frac{\langle u_z u_r \rangle}{r} \right] \langle u_z^3 \rangle = 0, \quad (1)$$

$$-\left[\frac{d\langle u_r^5 \rangle}{dr} + \frac{\langle u_r^5 \rangle}{r} - 4 \frac{\langle u_r^3 u_\varphi^2 \rangle}{r} \right] + 8 \langle u_r^3 u_\varphi \rangle \frac{U_\varphi}{r} + \Pi_{rr}^4 - \varepsilon_{rr}^4 + \nu \left[\nabla^2 \langle u_r^4 \rangle - 4 \frac{\langle u_r^4 \rangle}{r^2} \right] + 4 \left[\frac{d\langle u_r^2 \rangle}{dr} + \frac{\langle u_r^2 \rangle - \langle u_\varphi^2 \rangle}{r} \right] \langle u_r^3 \rangle = 0, \quad (2)$$

$$-\left[\frac{d\langle u_\varphi^4 u_r \rangle}{dr} + 5 \frac{\langle u_\varphi^4 u_r \rangle}{r} \right] - 4 \langle u_\varphi^3 u_r \rangle \left[\frac{dU_\varphi}{dr} + \frac{U_\varphi}{r} \right] + \Pi_{\varphi\varphi}^4 - \varepsilon_{\varphi\varphi}^4 + \nu \left[\nabla^2 \langle u_\varphi^4 \rangle - 4 \frac{\langle u_\varphi^4 \rangle}{r^2} \right] + 4 \left[\frac{d\langle u_r u_\varphi \rangle}{dr} + 2 \frac{\langle u_r u_\varphi \rangle}{r} \right] \langle u_\varphi^3 \rangle = 0, \quad (3)$$

where ν is the kinematic coefficient of molecular viscosity, and $\nabla^2 \equiv \frac{1}{r} \frac{\partial}{\partial r} \left(r \frac{\partial}{\partial r} \right) + \frac{1}{r^2} \frac{\partial^2}{\partial \varphi^2} + \frac{\partial^2}{\partial z^2}$ is the Laplace operator in the cylindrical coordinate system (for a steady-state fully developed turbulent flow in a pipe, this operator depends only on the radial coordinate r).

In equations (1)–(3), the correlations between the pressure and velocity pulsations have the form

$$\Pi_{zz}^4 \equiv -\frac{1}{\rho} \left\langle u_z^3 \frac{\partial p}{\partial z} \right\rangle, \quad \Pi_{rr}^4 \equiv -\frac{1}{\rho} \left\langle u_r^3 \frac{\partial p}{\partial r} \right\rangle, \quad (4)$$

$$\Pi_{\varphi\varphi}^4 \equiv -\frac{1}{r\rho} \left\langle u_\varphi^3 \frac{\partial p}{\partial \varphi} \right\rangle.$$

According to (A1), the components of the viscous dissipation tensor appearing in equations (1)–(3) will be written in the form

$$\varepsilon_{zz}^4 \equiv 12\nu \left\langle u_z^2 \left[\left(\frac{\partial u_z}{\partial z} \right)^2 + \left(\frac{\partial u_z}{\partial r} \right)^2 \right] \right\rangle,$$

$$\varepsilon_{rr}^4 \equiv 12\nu \left\langle u_r^2 \left[\left(\frac{\partial u_r}{\partial z} \right)^2 + \left(\frac{\partial u_r}{\partial r} \right)^2 \right] \right\rangle, \quad (5)$$

$$\varepsilon_{\varphi\varphi}^4 \equiv 12\nu \left\langle u_\varphi^2 \left[\left(\frac{\partial u_\varphi}{\partial z} \right)^2 + \left(\frac{\partial u_\varphi}{\partial r} \right)^2 \right] \right\rangle.$$

In what follows, we consider a steady-state turbulent flow in a straight round pipe at high Reynolds numbers. The latter assumption means that, in (1)–(3), the terms describing molecular transport will be neglected for being small compared to the similar terms describing turbulent transfer. In this case, the wall flow region is not included in the region under study. Such limitation is determined by the desire to obtain a gradient transfer model for the central fourth-order one-point moments. Besides, the third-order moments appearing in equations (1)–(3) are also found from the gradient transfer model that was constructed for the case of high Reynolds numbers [6, 7].

From equations (1)–(3), it follows that, to obtain their closed form, we need some model representations for describing turbulent transfer (the fifth-order moments) and the exchange processes affected by pressure pulsations (4), and processes of viscous dissipation (5).

2.1. A Model for Describing the Behavior of Higher-Order Moments in Equations (1)–(3)

In equations (1)–(3), the turbulent diffusion of the fourth-order moments is described by the fifth-order moments $\langle u_z^4 u_r \rangle$, $\langle u_r^5 \rangle$, $\langle u_r^3 u_\varphi^2 \rangle$, and $\langle u_\varphi^4 u_r \rangle$. To obtain a closed form of (1)–(3), we must express these fifth-order moments through lower-order moments.

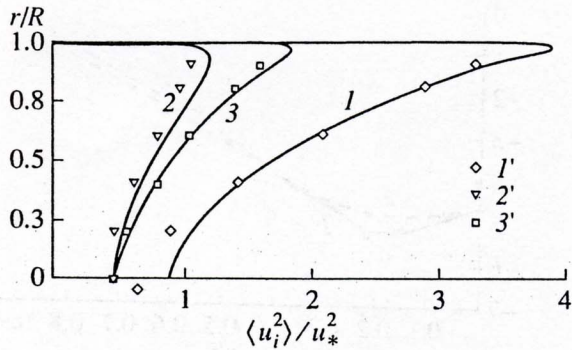


Fig. 1. Profiles of normal Reynolds stresses: (1, 1') $\langle u^2 \rangle$; (2, 2') $\langle v^2 \rangle$; (3, 3') $\langle w^2 \rangle$; (1'–3'), experimental data [12, 13]; and (1–3), computational results [6, 7].

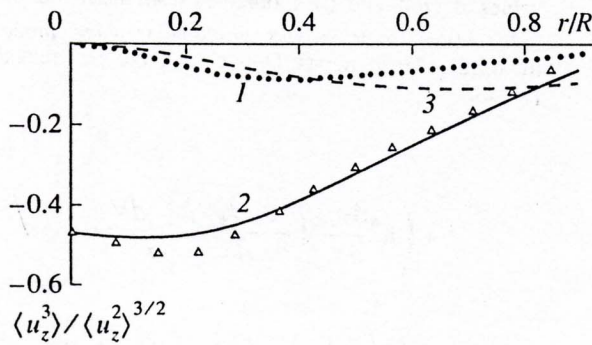


Fig. 2. Profile of the longitudinal asymmetry coefficient: (1) calculated by the simplified model (see text); (2) calculated by the full model [6, 7]; and (3) calculated by the Daly–Harlow model [15]. Delta points show the experimental data [13].

The experimental data [9] show that, in a fully developed flow in a round pipe, the probability density of the turbulent velocity field has a non-Gaussian form. Hence, according to [10], we can describe the turbulent velocity field by a combined two-dimensional Gram–Charlier-type probability density, i.e., represent the probability density function in the form of a series in Hermite polynomials with respect to a normal distribution. The fourth-order termination of such a series expansion (see also [11]) yields the expressions relating the fifth-order moments with the lower-order moments

$$\langle u_z^4 u_r \rangle = 6 \langle u_z^2 \rangle \langle u_z^2 u_r \rangle + 4 \langle u_z^3 \rangle \langle u_z u_r \rangle,$$

$$\langle u_r^5 \rangle = 10 \langle u_r^2 \rangle \langle u_r^3 \rangle, \tag{6}$$

$$\langle u_\phi^4 u_r \rangle = 6 \langle u_\phi^2 \rangle \langle u_\phi^2 u_r \rangle + 4 \langle u_\phi^3 \rangle \langle u_\phi u_r \rangle,$$

$$\langle u_\phi^2 u_r^3 \rangle = 6 \langle u_r u_\phi \rangle \langle u_r^2 u_\phi \rangle + 3 \langle u_r^2 \rangle \langle u_r u_\phi^2 \rangle + \langle u_\phi^2 \rangle \langle u_r^3 \rangle.$$

Note that, for the turbulent velocity field in a plane turbulent boundary layer bounded by a smooth solid surface, the convergence of the Gram–Charlier series expansion of the probability density function was proved experimentally [11].

In (6), the underlined terms are nonzero only for a fully developed turbulent flow in a round pipe rotating about its longitudinal axis. For a nonrotating turbulent flow, the correlation $\langle u_r u_\phi \rangle = 0$, and the first term in the right-hand part of the last expression (6) is also zero.

The experimental data on the behavior of the higher order moments (including those involved in (6)) of a fully developed flow in a round pipe are very limited. Therefore, these data allow no reliable verification of relations (6). However, the correctness of these relations may be estimated for the central fifth-order moment measured in [9, 12]. The central moments of the second and third orders were measured in [12–14]. Thus, we can directly verify the validity of the relation

$$\langle u_z^5 \rangle = 10 \langle u_z^3 \rangle \langle u_z^2 \rangle. \tag{7}$$

Figure 1 shows the profiles of the eddy kinetic energy in a fully developed turbulent flow in a straight round pipe. The dots show the experimental data [12, 13], and the solid lines show the computational results obtained from the model of Reynolds stress transfer [5–7]. Figure 2 shows the profiles of the longitudinal asymmetry coefficient (the normalized value of the third-order central moment for the longitudinal velocity pulsation) measured in the experiments [13] (delta points) and the corresponding profiles calculated by the gradient transfer models [6, 7]. The solid line shows the results of calculations performed by the full gradient transfer model. These results were obtained from the transfer equation for triple velocity correlations on the assumption that only the advection terms are negligibly small. The dotted line gives the results of calculations by a simplified gradient transfer model

$$\begin{aligned} -\langle u_i u_j u_k \rangle &= c_s^* \frac{E}{\epsilon} [\langle u_i u_j \rangle_{,m} \langle u^m u_k \rangle \\ &+ \langle u_j u_k \rangle_{,m} \langle u^m u_i \rangle + \langle u_k u_i \rangle_{,m} \langle u^m u_j \rangle] \\ (c_s^* &= 0.13). \end{aligned}$$

The dashed line in Fig. 2 shows the profile calculated by the simplest gradient transfer model [15] that was used in constructing the model of Reynolds stress transfer [6, 7]. The experimental data shown in Figs. 1 and 2 for $\langle u_z^2 \rangle$ and $\langle u_z^3 \rangle$ allowed us to calculate the profile of $\langle u_z^5 \rangle$ by relation (7) and compare it to the profile measured in the experiment. Such comparison is presented in Fig. 3. One can see that relation (7) agrees well with the experimental data. In this figure, the dashed line shows the computational results obtained by formula (7) with the values of $\langle u_z^2 \rangle$ and $\langle u_z^3 \rangle$ calculated by the model of Reynolds stress transfer and the gradient transfer model for the third moments [6, 7].

The distributions of these two quantities are shown by the solid lines in Figs. 1 and 2.

Although we successfully verified relation (7), relations (6) should be treated in our subsequent calculations as a hypothesis.

In (1) and (3), the generation of turbulence due to the average velocity shift is described by the terms

$$P_{zr}^4 = -4 \langle u_z^3 u_r \rangle \frac{dU_z}{dr},$$

$$P_{r\phi}^4 = -4 \langle u_\phi^3 u_r \rangle \left[\frac{dU_\phi}{dr} + \frac{U_\phi}{r} \right] \quad (8)$$

that involve mixed fourth-order moments. In equation (2), a mixed fourth-order moment enters the term containing the velocity U_ϕ . In the system of equations (1)–(3), these moments should be treated as the sought-for functions, for which the appropriate additional balance equations should be written. Analysis of this approach has showed that it requires treatment of other mixed fourth-order (and fifth-order) moments that do not appear in system (1)–(3). In principle, the fifth-order (and sixth-order) moments that appear in these additional equations may be expressed through the lower-order moments by relations similar to (6). However, because no experimental data are available on the behavior of these “additional” sought-for higher-order moments, complementing the system of equations (1)–(3) with balance equations is ineffective. Therefore, for the mixed fourth-order moments in (2) and (8), we use the expressions that comply with the Millionschikov hypothesis [2]

$$\langle u_z^3 u_r \rangle = 3 \langle u_z^2 \rangle \langle u_z u_r \rangle,$$

$$\langle u_r^3 u_\phi \rangle = 3 \langle u_r^2 \rangle \langle u_r u_\phi \rangle,$$

$$\langle u_\phi^3 u_r \rangle = 3 \langle u_\phi^2 \rangle \langle u_\phi u_r \rangle.$$

2.2. Model Expressions for the Exchange Processes Caused by Pressure Pulsations and Viscous Dissipation

In [16], it has been shown that, by using a specific solution to the Poisson equation for pressure pulsations, it is possible to derive an exact formula for the correlations between the pressure and velocity pulsations in the transfer equations for Reynolds stresses and third-order moments of the velocity field.

For the central $(n + 1)$ -order moments satisfying the exact nonclosed equation (A1), the exact expression for the correlation $\Pi_{ii}^{n+1} = -(1/\rho) \langle u_i^n p_i \rangle$ has the form

$$\Pi_{ii}^{n+1}(\mathbf{x}) = -\frac{1}{4\pi} \int_V \left[\left\langle u_i^n \frac{\partial^2 u_i'}{\partial x_i \partial x_k} \right\rangle \left(\frac{\partial U_k}{\partial x_m} \right)' \right] dV,$$

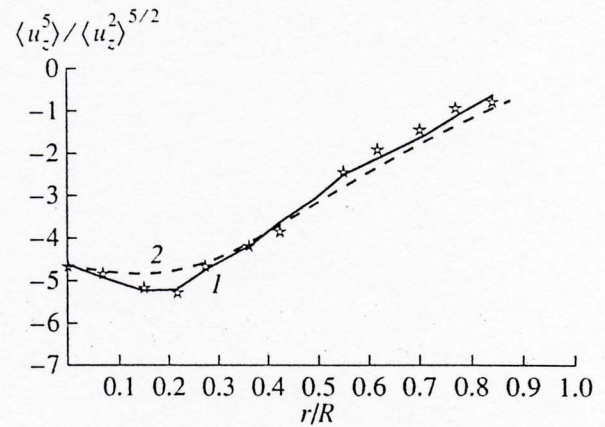


Fig. 3. Profile of the fifth-order moment $\langle u_z^5 \rangle / \langle u_z^2 \rangle^{5/2}$: (1) calculated by model (7); (2) calculated by (7) with the values of $\langle u_z^2 \rangle$ and $\langle u_z^3 \rangle$ obtained from the model of Reynolds stress transfer and gradient transfer model for the third-order moments. Dots show the experimental data [9, 12].

$$+ \left\langle u_i^n \frac{\partial u_m}{\partial x_k} \right\rangle \left(\frac{\partial^2 U_k}{\partial x_i \partial x_m} \right)' \Big|_{|\mathbf{x} - \mathbf{y}|} \quad (9)$$

$$- \int_V \left[\left\langle u_i^n \right\rangle \frac{\partial^3 \langle u_k' u_m' \rangle}{\partial x_i \partial x_k \partial x_m} - \left\langle u_i^n \frac{\partial^3 u_k' u_m'}{\partial x_i \partial x_k \partial x_m} \right\rangle \right] \Big|_{|\mathbf{x} - \mathbf{y}|} dV,$$

where the terms with and without prime are calculated at the points \mathbf{y} and \mathbf{x} , respectively, and the integration is performed with respect to \mathbf{y} . For the central fourth-order moments, we assume that, in formula (9), $n = 3$.

Like similar expressions in the transfer equations for the second and third moments of the velocity field (see, e.g., [5–7] and [16]), expression (9) involves two groups of terms. One group ($\Pi_{ii,1}^{n+1}$) describes the nonlinear interaction between the velocity pulsations, and the other ($\Pi_{ii,2}^{n+1}$) describes the effect of the average velocity shift.

In [17], it was shown that, to simulate the correlations between the pressure and the second-order velocity shift in the transfer equation for Reynolds stress, it is possible to perform the individual simulations of the above-mentioned groups of terms. In this case, the resulting expression obtained for this correlation has the form of the sum of two terms, one of which describes the energy exchange between the differently directed pulsations (“tendency toward isotropy”) and the other describes the interaction between the field of velocity pulsations and the average velocity shift (the so-called “fast terms”).

We use this approach to simulate the correlation under study in the form $\Pi_{ii}^4(\mathbf{x}) = \Pi_{ii,1}^4 + \Pi_{ii,2}^4$. For the

first part of the correlation $\Pi_{ii,1}^4$ ("tendency toward isotropy"), we write the expression

$$\Pi_{ii,1}^4 = -c_{14} \frac{\varepsilon}{E} [\langle u_i^4 \rangle - 3 \langle u_i^2 \rangle^2], \quad (10)$$

where c_{14} is an empirical numerical coefficient, $E = \langle u_i u_i \rangle / 2$ is the eddy kinetic energy density (per unit mass), and ε characterizes the dissipation of the eddy energy (no summation over i is performed). Expression (10) is constructed on the basis of the experimental data (see, e.g., [1, ch. 7]). It was found that, for the large-scale components of turbulent motion observed at the initial stage of decay of homogeneous and isotropic turbulence behind the honeycomb in a wind tunnel, a fourth-order one-point moment of the velocity field satisfies the relation

$$\langle u_i^4 \rangle - 3 \langle u_i^2 \rangle^2 = 0 \quad (i = 1, 2, 3) \quad (11)$$

within the measurement error (not exceeding 10% of the measured values). This relation represents a specific case of the Millionshchikov hypothesis [2] expressed by the equation

$$\begin{aligned} \langle u_i u_j u_m u_n \rangle &= \langle u_i u_j \rangle \langle u_m u_n \rangle \\ &+ \langle u_i u_m \rangle \langle u_j u_n \rangle + \langle u_i u_n \rangle \langle u_j u_m \rangle. \end{aligned}$$

From the experimental studies of flow in a wind tunnel behind the honeycomb [10], it has been found that the behavior of the mixed fourth-order moments of the velocity field complies (within the limits of measurement error) with the Gaussian distribution of the combined probability density of the turbulent velocity field.

Hence, relation (10) approximately describes the "limiting" state of homogeneous and isotropic turbulence in the flow behind the honeycomb, for which a part of correlation $\Pi_{ii,1}^4$ is zero.

To obtain a model expression for the second part of the correlation $\Pi_{ii,2}^4$, we use the above-mentioned experimental data [10] to write the general tensor expression for the fourth-order correlation between the pressure and velocity pulsations

$$\begin{aligned} \Pi_{ijmn}^4 &= -c_{14} \frac{\varepsilon}{E} [\langle u_i u_j u_m u_n \rangle - (\langle u_i u_j \rangle \langle u_m u_n \rangle \\ &+ \langle u_i u_m \rangle \langle u_j u_n \rangle + \langle u_i u_n \rangle \langle u_j u_m \rangle)] + a_{ijmnl} \frac{\partial U^k}{\partial x_l}. \end{aligned} \quad (12)$$

In this expression, the second term describes the effect of the average velocity shift on the turbulence. This term is written on the basis of the assumptions that were used in [17] for describing a similar correlation in the equation for the Reynolds stress tensor. In (12), the quantity a_{ijmnl} is a sixth-order tensor function of the fourth-order moments and Reynolds stresses. Without

presenting the cumbersome general form of this function, we only note that it involves ten arbitrary coefficients. The conditions of mass conservation and symmetry provide four relations between these coefficients. However, because of the absence of the required experimental data on the higher-order moments of the velocity field, we cannot determine the numerical values of these coefficients in the same way as it was done for the correlation between the pressure and the velocity shift in the equation for the Reynolds stress tensor (see, e.g., [18]).

For an incompressible turbulent flow dominated by only one component of the mean velocity shift (parabolic-type boundary layer flow), we can write the model expressions for the components of the part of correlation $\Pi_{ii,2}^4$ by using the general form of the tensor function

$$\begin{aligned} \Pi_{zz,2}^4 &= -c_{24} E P_{zr} - c_{34} E P_{r\varphi}, \\ \Pi_{rr,2}^4 &= -c'_{24} E P_{zr} - c'_{34} E P_{r\varphi}, \\ \Pi_{\varphi\varphi,2}^4 &= -c''_{24} E P_{zr} - c''_{34} E P_{r\varphi}. \end{aligned} \quad (13)$$

Here, $P_{zr} = -\langle u_z u_r \rangle (dU_z/dr)$, $P_{r\varphi} = -\langle u_r u_\varphi \rangle dU_\varphi/dr$ describes the turbulence generation due to the mean velocity shift, and c_{24} , c'_{24} , c''_{24} , c_{34} , c'_{34} , and c''_{34} are empirical coefficients.

By combining expressions (10) and (13), we derive the following model expressions for the components of the fourth-order correlation between the pressure and velocity pulsations in the cylindrical coordinate system:

$$\begin{aligned} \Pi_{zz}^4 &= -c_{14} \frac{\varepsilon}{E} [\langle u_z^4 \rangle - 3 \langle u_z^2 \rangle^2] \\ &\quad - c_{24} E P_{zr} - c_{34} E P_{r\varphi}, \\ \Pi_{rr}^4 &= -c_{14} \frac{\varepsilon}{E} [\langle u_r^4 \rangle - 3 \langle u_r^2 \rangle^2] \\ &\quad - c'_{24} E P_{zr} - c'_{34} E P_{r\varphi}, \\ \Pi_{\varphi\varphi}^4 &= -c_{14} \frac{\varepsilon}{E} [\langle u_\varphi^4 \rangle - 3 \langle u_\varphi^2 \rangle^2] \\ &\quad - c''_{24} E P_{zr} - c''_{34} E P_{r\varphi}. \end{aligned} \quad (14)$$

To estimate the contribution of viscous dissipation to the transfer equations for the central fourth-order moments (1)–(3), i.e., to estimate the terms ε_{zz}^4 , ε_{rr}^4 , and $\varepsilon_{\varphi\varphi}^4$, we used a gradient transfer model similar to

that used in [6, 7] for describing the triple velocity correlations. This model has the form

$$\begin{aligned} \epsilon_{ijkm} = & -c_{E4} \frac{E}{\epsilon} \left[\langle u_i u_j u_l \rangle \frac{\partial \epsilon_{km}}{\partial x_l} + \langle u_i u_k u_l \rangle \frac{\partial \epsilon_{jm}}{\partial x_l} \right. \\ & + \langle u_i u_m u_l \rangle \frac{\partial \epsilon_{jk}}{\partial x_l} + \langle u_j u_k u_l \rangle \frac{\partial \epsilon_{im}}{\partial x_l} \\ & \left. + \langle u_j u_m u_l \rangle \frac{\partial \epsilon_{ik}}{\partial x_l} + \langle u_k u_m u_l \rangle \frac{\partial \epsilon_{ij}}{\partial x_l} \right]. \end{aligned} \quad (15)$$

Here, ϵ_{ij} is the viscous dissipation tensor in the transfer equation of Reynolds stress, and c_{E4} is an empirical numerical coefficient.

For turbulent flow in a straight round pipe, the terms describing viscous destruction in equations (1)–(3) can be written according to (15) in the form

$$\begin{aligned} \epsilon_{zz}^4 = & -6c_{E4} \frac{E}{\epsilon} \langle u_z^2 u_r \rangle \frac{d\epsilon_{zz}}{dr}, \\ \epsilon_{rr}^4 = & -6c_{E4} \frac{E}{\epsilon} \langle u_r^3 \rangle \frac{d\epsilon_{rr}}{dr}, \\ \epsilon_{\varphi\varphi}^4 = & -6c_{E4} \frac{E}{\epsilon} \langle u_\varphi^2 u_r \rangle \left(\frac{d\epsilon_{\varphi\varphi}}{dr} - \frac{2\epsilon_{\varphi\varphi}}{r} \right) \frac{1}{r^2}, \end{aligned} \quad (16)$$

where $\epsilon_{zz} = \langle u_z^2 \rangle \frac{\epsilon}{E}$, $\epsilon_{rr} = \langle u_r^2 \rangle \frac{\epsilon}{E}$, and $\epsilon_{\varphi\varphi} = \langle u_\varphi^2 \rangle r^2 \frac{\epsilon}{E}$ are anisotropic expressions for the tensor components describing the viscous dissipation of normal Reynolds stresses. Substitution of expressions (14) and (16) into the balance equations for the central fourth-order moments (1)–(3) yields a gradient transfer model that allows the description of the central fourth-order one-point moments in a fully developed turbulent flow in a straight round pipe in the case of high Reynolds numbers

$$\begin{aligned} \langle u_z^4 \rangle - 3\langle u_z^2 \rangle^2 = & \frac{1}{c_{14}} \frac{E}{\epsilon} \left[-6\langle u_z^2 \rangle \left(\frac{d\langle u_z^2 u_r \rangle}{dr} + \frac{\langle u_z^2 u_r \rangle}{r} \right) \right. \\ & - 6\langle u_z^2 u_r \rangle \frac{d\langle u_z^2 \rangle}{dr} - 4\langle u_z u_r \rangle \frac{d\langle u_z^3 \rangle}{dr} \\ & + (12\langle u_z^2 \rangle - c_{24}E)P_{zr} - c_{34}EP_{r\varphi} \\ & \left. + 6c_{E4} \frac{E}{\epsilon} \langle u_z^2 u_r \rangle \frac{d}{dr} \left(\langle u_z^2 \rangle \frac{\epsilon}{E} \right) \right], \\ \langle u_r^4 \rangle - 3\langle u_r^2 \rangle^2 = & \frac{1}{c_{14}} \frac{E}{\epsilon} \left[-6\langle u_r^3 \rangle \left(\frac{d\langle u_r^2 \rangle}{dr} + \frac{\langle u_r^2 \rangle}{r} \right) \right. \\ & - 10\langle u_r^2 \rangle \frac{d\langle u_r^3 \rangle}{dr} + 12\langle u_r^2 \rangle \frac{\langle u_r u_\varphi^2 \rangle}{r} - c_{24}''EP_{zr} \end{aligned} \quad (17)$$

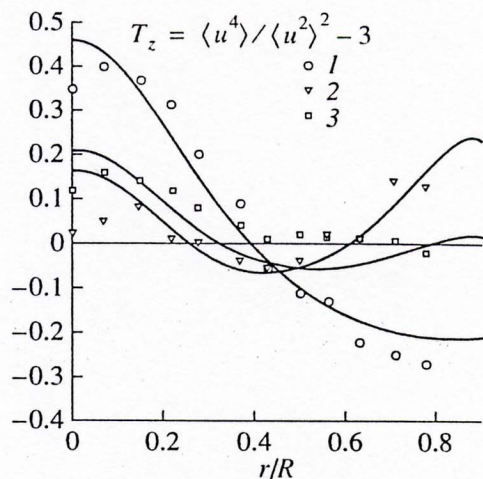


Fig. 4. Profiles of the longitudinal coefficient of excess. Experimental data [12–14]: (1) $P = 0$; (2) $P = 0.65$; (3) $P = 0.47$. Solid lines show the computational results obtained from model (17).

$$\begin{aligned} -c_{34}'EP_{r\varphi} + 24\langle u_r^2 \rangle \langle u_r u_\varphi \rangle \frac{U_\varphi}{r} \\ + 6c_{E4} \frac{E}{\epsilon} \langle u_r^3 \rangle \frac{d}{dr} \left(\langle u_r^2 \rangle \frac{\epsilon}{E} \right) \end{aligned}$$

$$\begin{aligned} \langle u_\varphi^4 \rangle - 3\langle u_\varphi^2 \rangle^2 = & \frac{1}{c_{14}} \frac{E}{\epsilon} \left[-6\langle u_\varphi^2 \rangle \left(\frac{d\langle u_\varphi^2 u_r \rangle}{dr} + 5\frac{\langle u_\varphi^2 u_r \rangle}{r} \right) \right. \\ & - 6\langle u_\varphi^2 u_r \rangle \frac{d\langle u_\varphi^2 \rangle}{dr} - 12\langle u_\varphi^2 \rangle \langle u_r u_\varphi \rangle \left(\frac{dU_\varphi}{dr} + \frac{U_\varphi}{r} \right) \\ & \left. - c_{24}''EP_{zr} - c_{34}''EP_{r\varphi} + 6c_{E4} \frac{E}{\epsilon} \langle u_\varphi^2 u_r \rangle \frac{d}{dr} \left(\langle u_\varphi^2 \rangle \frac{\epsilon}{E} \right) \right]. \end{aligned}$$

Because of the lack of experimental data about the terms representing viscous destruction ϵ_{zz}^4 , ϵ_{rr}^4 , and $\epsilon_{\varphi\varphi}^4$, an independent determination of the coefficient c_{E4} is impossible.

The numerical values of the coefficients involved in (14) are found from the comparison of the coefficients of excess $T_z \equiv \langle u_z^4 \rangle / \langle u_z^2 \rangle^2 - 3$, $T_r \equiv \langle u_r^4 \rangle / \langle u_r^2 \rangle^2 - 3$, and $T_\varphi \equiv \langle u_\varphi^4 \rangle / \langle u_\varphi^2 \rangle^2$, calculated from (17) for the turbulent velocity field, with the experimental data (see below in Section 3, Figs. 4–6): $c_{14} = 18.0$; $c_{24} = 17.0$; $c_{24}' = c_{24}'' = -0.7$; $c_{E4} = 0.1$; $c_{34} = -50.0$; $c_{34}' = -0.7$; and $c_{34}'' = -3.0$.

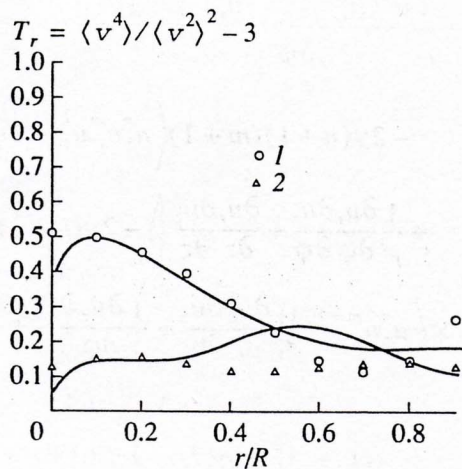


Fig. 5. Profiles of the radial coefficient of excess. Experimental data [12–14]: (1) $P = 0$; (2) $P = 0.60$. Solid lines show the computational results obtained from model (17).

3. RESULTS OBTAINED BY SIMULATING THE BEHAVIOR OF THE COEFFICIENTS OF EXCESS FOR A FULLY DEVELOPED TURBULENT FLOW IN A ROUND PIPE

The profiles of the coefficients of excess $T_z \equiv \langle u_z^4 \rangle / \langle u_z^2 \rangle^2 - 3$, $T_r \equiv \langle u_r^4 \rangle / \langle u_r^2 \rangle^2 - 3$, and $T_\varphi \equiv \langle u_\varphi^4 \rangle / \langle u_\varphi^2 \rangle^2 - 3$, calculated from gradient transfer model (17), are given in Figs. 4–6. The required values of the second- and third-order moments involved in the right-hand parts of equations (17) were obtained by successive realization of the model of Reynolds stress transfer [5–7] and the gradient transfer model for triple velocity correlations [6, 7]. In Figs. 4–6, the computational results (solid lines) are correlated with the experimental data (dots) [12–14]. For a nonswirling flow, the distributions of the coefficients of excess were calculated by formulas (17) assuming that $U_\varphi = 0$ ($P_{r\varphi} = 0$). The calculated distributions of the coefficients of excess appear in adequate agreement with their measured values over the entire cross section of the tube, except for the wall region of flow, where model (17) is invalid. We note that the gradient transfer model proposed in [6, 7] for describing the triple velocity correlations was also formulated for large Reynolds numbers, and its range of validity does not cover the entire wall region. The calculated profile of excess T_r , markedly deviates from the corresponding experimental data for the parameter of flow swirling $P = 0.6$ in the region $0.35 < r/R < 0.8$. (The parameter P is defined as $P \equiv U_\varphi/U_0 = \omega_0 R/U_0$, where ω_0 is the rate of pipe rotation, U_0 is the flow velocity at the pipe axis, and R is the pipe radius.) This distinction is associated with the fact that the models of turbulent transfer of the second and third moments [6] only qualitatively reproduce the profile of radial asymmetry of the turbulent velocity field for the flow with the parameter of flow swirling $P = 0.6$ (see Fig. 8 in [6]).

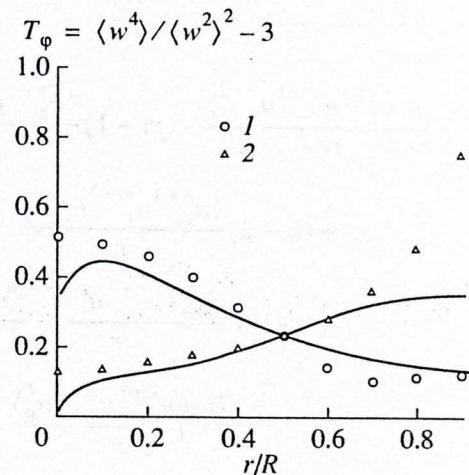


Fig. 6. Profiles of the angular coefficient of excess. Experimental data [12–14]: (1) $P = 0$; (2) $P = 0.60$. Solid lines show the computational results obtained from model (17).

Note that the results obtained from model (17) are presented in the form of the excess, which is a more detailed characteristic of the flow than the related kurtosis characteristic ($\langle u_i^4 \rangle / \langle u_i^2 \rangle^2$).

Note further that the calculated profiles of the coefficients of excess T_z , T_r and T_φ shown in Figs. 4–6 were obtained from the full model (14) for the correlation Π_{ii}^4 . If, in (14), the part of correlation $\Pi_{ii,2}^4$ describing the effect of the mean velocity shift is neglected, the computational results will only qualitatively agree with the experimental data for all three coefficients of excess.

ACKNOWLEDGMENTS

This study was supported by the Russian Foundation for Basic Research (project no. 94-05-16287). S.V. Poroseva acknowledges the support of the International Program on Education in Exact Sciences (the Soros Postgraduate subprogram, grant no. 96-02-16001).

APPENDIX

Below, we have written the exact nonclosed equation for the mixed moment $\langle u_z^{n+1} u_r^{m+1} u_\varphi^{k+1} \rangle$ in the cylindrical coordinate system. The equation was obtained from the Navier–Stokes and Reynolds equations by using a conventional procedure (see the beginning of Section 2).

$$\begin{aligned} & \frac{\partial \langle u_z^{n+1} u_r^{m+1} u_\varphi^{k+1} \rangle}{\partial t} + U_r \frac{\partial \langle u_z^{n+1} u_r^{m+1} u_\varphi^{k+1} \rangle}{\partial r} \\ & + U_\varphi \frac{\partial \langle u_z^{n+1} u_r^{m+1} u_\varphi^{k+1} \rangle}{r \partial \varphi} + U_z \frac{\partial \langle u_z^{n+1} u_r^{m+1} u_\varphi^{k+1} \rangle}{\partial z} \end{aligned}$$

$$\begin{aligned}
 & + \frac{\partial \langle u_z^{n+1} u_r^{m+2} u_\varphi^{k+1} \rangle}{\partial r} + \frac{\partial \langle u_z^{n+2} u_r^{m+1} u_\varphi^{k+1} \rangle}{\partial z} \\
 & + \frac{\partial \langle u_z^{n+1} u_r^{m+1} u_\varphi^{k+2} \rangle}{r \partial \varphi} - (m+1) \frac{\langle u_z^{n+1} u_r^m u_\varphi^{k+3} \rangle}{r} \\
 & + (k+2) \frac{\langle u_z^{n+1} u_r^{m+2} u_\varphi^{k+1} \rangle}{r} \\
 & - (m+1) \frac{2U_\varphi \langle u_z^{n+1} u_r^m u_\varphi^{k+2} \rangle}{r} \\
 & + (k+1) \frac{U_\varphi \langle u_z^{n+1} u_r^{m+2} u_\varphi^k \rangle}{r} \\
 & + (n-k) \langle u_z^{n+1} u_r^{m+1} u_\varphi^{k+1} \rangle \frac{\partial U_z}{\partial z} \\
 & + (m-k) \langle u_z^{n+1} u_r^{m+1} u_\varphi^{k+1} \rangle \frac{\partial U_r}{\partial r} \\
 & + (n+1) \left[\langle u_z^n u_r^{m+2} u_\varphi^{k+1} \rangle \frac{\partial U_z}{\partial r} + \frac{\langle u_z^n u_r^{m+1} u_\varphi^{k+2} \rangle}{r} \frac{\partial U_z}{\partial \varphi} \right] \\
 & + (m+1) \left[\langle u_z^{n+2} u_r^m u_\varphi^{k+1} \rangle \frac{\partial U_r}{\partial z} + \frac{\langle u_z^{n+1} u_r^m u_\varphi^{k+2} \rangle}{r} \frac{\partial U_r}{\partial \varphi} \right] \\
 & + (k+1) \left[\langle u_z^{n+1} u_r^{m+2} u_\varphi^k \rangle \frac{\partial U_\varphi}{\partial r} + \langle u_z^{n+2} u_r^{m+1} u_\varphi^k \rangle \frac{\partial U_\varphi}{\partial z} \right] \\
 & - (n+1) \langle u_z^n u_r^{m+1} u_\varphi^{k+1} \rangle \left[\frac{\partial \langle u_z u_r \rangle}{\partial r} + \frac{1}{r} \frac{\partial \langle u_z u_\varphi \rangle}{\partial \varphi} \right. \\
 & \left. + \frac{\partial \langle u_z^2 \rangle}{\partial z} + \frac{\langle u_z u_r \rangle}{r} \right] - (m+1) \langle u_z^{n+1} u_r^m u_\varphi^{k+1} \rangle \left[\frac{\partial \langle u_r^2 \rangle}{\partial r} \right. \\
 & \left. + \frac{1}{r} \frac{\partial \langle u_r u_\varphi \rangle}{\partial \varphi} + \frac{\partial \langle u_z u_r \rangle}{\partial z} + \frac{\langle u_r^2 \rangle - \langle u_\varphi^2 \rangle}{r} \right] \\
 & - (k+1) \langle u_z^{n+1} u_r^{m+1} u_\varphi^k \rangle \left[\frac{\partial \langle u_r u_\varphi \rangle}{\partial r} + \frac{1}{r} \frac{\partial \langle u_\varphi^2 \rangle}{\partial \varphi} \right. \\
 & \left. + \frac{\partial \langle u_z u_\varphi \rangle}{\partial z} + \frac{2 \langle u_r u_\varphi \rangle}{r} \right] = - \frac{(n+1)}{\rho} \left\langle u_z^n u_r^{m+1} u_\varphi^{k+1} \frac{\partial p}{\partial z} \right\rangle \\
 & - \frac{(m+1)}{\rho} \left\langle u_z^{n+1} u_r^m u_\varphi^{k+1} \frac{\partial p}{\partial r} \right\rangle \\
 & - \frac{(k+1)}{r \rho} \left\langle u_z^{n+1} u_r^{m+1} u_\varphi^k \frac{\partial p}{\partial \varphi} \right\rangle \\
 & + \nu \left[\frac{\partial^2 \langle u_z^{n+1} u_r^{m+1} u_\varphi^{k+1} \rangle}{\partial r^2} + \frac{\partial^2 \langle u_z^{n+1} u_r^{m+1} u_\varphi^{k+1} \rangle}{\partial z^2} \right]
 \end{aligned}$$

$$\begin{aligned}
 & + \frac{1}{r^2} \frac{\partial^2 \langle u_z^{n+1} u_r^{m+1} u_\varphi^{k+1} \rangle}{\partial \varphi^2} + \frac{1}{r} \frac{\partial \langle u_z^{n+1} u_r^{m+1} u_\varphi^{k+1} \rangle}{\partial r} \Bigg] \\
 & - 2\nu(n+1)(m+1) \left\langle u_z^n u_r^m u_\varphi^{k+1} \left[\frac{\partial u_r}{\partial r} \frac{\partial u_z}{\partial r} \right. \right. \\
 & \left. \left. + \frac{1}{r^2} \frac{\partial u_r}{\partial \varphi} \frac{\partial u_z}{\partial \varphi} + \frac{\partial u_r}{\partial z} \frac{\partial u_z}{\partial z} \right] \right\rangle - 2\nu(n+1)(k+1) \\
 & \times \left\langle u_z^n u_r^{m+1} u_\varphi^k \left[\frac{\partial u_\varphi}{\partial r} \frac{\partial u_z}{\partial r} + \frac{1}{r^2} \frac{\partial u_\varphi}{\partial \varphi} \frac{\partial u_z}{\partial \varphi} + \frac{\partial u_\varphi}{\partial z} \frac{\partial u_z}{\partial z} \right] \right\rangle \\
 & - 2\nu(k+1)(m+1) \\
 & \times \left\langle u_z^{n+1} u_r^m u_\varphi^k \left[\frac{\partial u_r}{\partial r} \frac{\partial u_\varphi}{\partial r} + \frac{1}{r^2} \frac{\partial u_r}{\partial \varphi} \frac{\partial u_\varphi}{\partial \varphi} + \frac{\partial u_r}{\partial z} \frac{\partial u_\varphi}{\partial z} \right] \right\rangle \\
 & - \nu n(n+1) \left\langle u_z^{n-1} u_r^{m+1} u_\varphi^{k+1} \left[\left(\frac{\partial u_z}{\partial r} \right)^2 + \frac{1}{r^2} \left(\frac{\partial u_z}{\partial \varphi} \right)^2 \right. \right. \\
 & \left. \left. + \left(\frac{\partial u_z}{\partial z} \right)^2 \right] \right\rangle - \nu m(m+1) \left\langle u_z^{n+1} u_r^{m-1} u_\varphi^{k+1} \left[\left(\frac{\partial u_r}{\partial r} \right)^2 \right. \right. \\
 & \left. \left. + \frac{1}{r^2} \left(\frac{\partial u_r}{\partial \varphi} \right)^2 + \left(\frac{\partial u_r}{\partial z} \right)^2 \right] \right\rangle - \nu k(k+1) \\
 & \times \left\langle u_z^{n+1} u_r^{m+1} u_\varphi^{k-1} \left[\left(\frac{\partial u_\varphi}{\partial r} \right)^2 + \frac{1}{r^2} \left(\frac{\partial u_\varphi}{\partial \varphi} \right)^2 + \left(\frac{\partial u_\varphi}{\partial z} \right)^2 \right] \right\rangle \\
 & - \frac{\nu(m+1)}{r^2} \langle u_z^{n+1} u_r^{m+1} u_\varphi^{k+1} \rangle \\
 & - \frac{2\nu(m+1)}{r^2} \left\langle u_z^{n+1} u_r^{m+1} u_\varphi^{k+1} \frac{\partial u_\varphi}{\partial \varphi} \right\rangle \\
 & - \frac{\nu(k+1)}{r^2} \langle u_z^{n+1} u_r^{m+1} u_\varphi^{k+1} \rangle \\
 & + \frac{2\nu(k+1)}{r^2} \left\langle u_z^{n+1} u_r^{m+1} u_\varphi^k \frac{\partial u_r}{\partial \varphi} \right\rangle.
 \end{aligned}$$

REFERENCES

1. Monin, A.S. and Yaglom, A.M., *Statisticheskaya gidromekhanika* (Statistical Hydromechanics), Moscow: Nauka, 1967, vol. 2.
2. Millionshchikov, M.D., *Dokl. Akad. Nauk SSSR*, 1941, vol. 32, no. 9, p. 611.
3. Uberoi, M.S., *J. Aero. Sci.*, 1953, vol. 20, no. 3, p. 197.
4. Zaets, P.G., Onufriev, A.T., Pilipchuk, M.I., and Safarov, R.A., *Dvukhtocheynye korrelyatsionnye funktsii chetvertogo poriyadka dlya prodol'noi skorosti v turbulentnom techenii vo vrashchayushchey otositel'no*

- osi trube* (Fourth-Order Two-Point Correlation Functions for the Longitudinal Velocity in a Turbulent Flow in a Tube Rotating about Its Axis), Available from VINITI, 1984, Moscow, no. 3831-84.
5. Zaets, P.G., Kurbatskii, A.F., Onufriev, A.T., Poroseva, S.V., Safarov, N.A., Safarov, R.A., and Yakovenko, S.N., *Russ. J. Comput. Mech.*, 1994, no. 4.
 6. Kurbatskii, A.F., Poroseva, S.V., and Yakovenko, S.N., *Teplofiz. Vys. Temp.*, 1995, vol. 33, no. 5, p. 738 [*High Temp.* (Engl. transl.), vol. 33, no. 5, p. 732].
 7. Kurbatskii, A.F., Poroseva, S.V., and Yakovenko, S.N., *ICAR Paper* no. 7-94 (Sci. Rep. Int. Center of Aerophys. Res., Inst. Theor. Appl. Mech., Russ. Acad. Sci., Siberian Division, Novosibirsk).
 8. Monin, A.S. and Yaglom, A.M., *Statisticheskaya gidromekhanika* (Statistical Hydromechanics), St. Petersburg: Gidrometeoizdat, 1992, vol. 1.
 9. Bukreev, V.I., Zykov, V.V., and Kostomakha, V.A., *Izv. Sib. Otd. Akad. Nauk SSSR, Ser. Tekh. Nauk*, 1975, no. 13, no. 3, p. 3.
 10. Frenkiel, F.N. and Klebanoff, P.S., *Phys. Fluids*, 1966, vol. 10, no. 3, p. 507.
 11. Jovanovic, J., Durst, F., and Johansson, T.G., *Phys. Fluids A*, 1993, vol. 5, no. 11, p. 2886.
 12. Pilipchuk, M.I., *Cand. Sci. (Phys.-Math.) Dissertatio* Moscow: Moscow Physicotechnical Inst., 1986.
 13. Zaets, P.G., Safarov, N.A., and Safarov, R.A., in *Sovremennye problemy mekhaniki sploshnykh sred* (Current Problems of Continuum Mechanics), Moscow: Moscow Fiz.-Tekh. Inst., 1985, p. 136.
 14. Safarov, N.A., *Cand. Sci. (Phys.-Math.) Dissertatio* Moscow: Moscow Physicotechnical Inst., 1986.
 15. Daly, B.J. and Harlow, F.H., *Phys. Fluids*, 1970, vol. 13, no. 11, p. 2634.
 16. Chou, P.Y., *Quart. Appl. Math.*, 1945, vol. 3, no. 1, p. 38.
 17. Rotta, J.C., *Z. Phys.*, 1951, vol. 129, no. 5, p. 547; vol. 131, no. 1, p. 51.
 18. Jones, W.P. and Musonge, P., *Phys. Fluids*, 1988, vol. 31, no. 12, p. 3589.